An uncommon neuronal class conveys visual signals from rods and cones to retinal ganglion cells

Brent K. Young[a,b], Charu Ramakrishnan[c], Tushar Ganjawala[d], Ping Wang[a], Karl Deisseroth[c,e], and Ning Tian[a,b,f,g,h,1]

[a]Department of Ophthalmology & Visual Sciences, University of Utah, Salt Lake City, UT 84132; [b]Interdepartmental Neuroscience Program, University of Utah, Salt Lake City, UT 84114; [c]Department of Bioengineering, Stanford University, Stanford, CA 94305; [d]Department of Ophthalmology, Visual and Anatomical Sciences, Wayne State University School of Medicine, Detroit, MI 48202; [e]Howard Hughes Medical Institute, Stanford University, Stanford, CA 94305; [f]Department of Neurobiology, University of Utah, Salt Lake City, UT 84132; [g]Department of Biomedical Engineering, University of Utah, Salt Lake City, UT 84132; and [h]Veterans Affairs Medical Center, Salt Lake City, UT 84148

Edited by Marla B. Feller, University of California, Berkeley, CA, and accepted by Editorial Board Member Jeremy Nathans September 7, 2021 (received for review April 8, 2021)

Neurons in the central nervous system (CNS) are distinguished by the neurotransmitter types they release, their synaptic connections, morphology, and genetic profiles. To fully understand how the CNS works, it is critical to identify all neuronal classes and reveal their synaptic connections. The retina has been extensively used to study neuronal development and circuit formation. Here, we describe a previously unidentified interneuron in mammalian retina. This interneuron shares some morphological, physiological, and molecular features with retinal bipolar cells, such as receiving input from photoreceptors and relaying visual signals to retinal ganglion cells. It also shares some features with amacrine cells (ACs), particularly Aii-ACs, such as their neurite morphology in the inner plexiform layer, the expression of some AC-specific markers, and possibly the release of the inhibitory neurotransmitter glycine. Thus, we unveil an uncommon interneuron, which may play an atypical role in vision.

retina cell class | glycinergic interneuron | bipolar cell | amacrine cell | transsynaptic

Photons entering the eye are detected by photoreceptors and processed through a set of function-specific synaptic pathways in the retina. The structural basis of these pathways are the synaptic connections among five major classes of retinal neurons: photoreceptors, horizontal cells (HCs), bipolar cells (BCs), amacrine cells (ACs), and retinal ganglion cells (RGCs) (1–3). Two fundamental features of the vertebrate retina's visual signal processing are the functional separation of scotopic and photopic vision (4–6) and the segregation of increment and decrement luminance signals into ON and OFF pathways (3, 7).

The functional separation of scotopic and photopic vision starts at rod and cone photoreceptors and remains separated at BCs through specific synaptic connections from rods to rod BCs and cones to cone BCs (3, 5, 8, 9). The segregation of increment and decrement luminance signals starts at BCs, where glutamate released from cones activates ionotropic glutamate receptors on the OFF cone BCs resulting in depolarization of the cell membrane potential (10). In contrast, glutamate activates a metabotropic glutamate receptor, mGluR6, on the rod BCs and ON cone BCs resulting in hyperpolarization of these cells (11–16). This sign reversing and nonreversing action of glutamate on the ON and OFF BCs separates the increment and decrement luminance signals into ON and OFF pathways, which remain segregated throughout the visual system (8, 17, 18). In the retina, BCs are thought to be the only interneuron to relay visual signals from photoreceptors to RGCs, and they are the primary excitatory driver for RGCs (19–22). All BCs have a dendrite in the outer plexiform layer (OPL) and axons in the inner plexiform layer (IPL), except for a recently identified monopolar interneuron (23). Additionally, it is commonly assumed that all BC types have been identified in the mouse retina (7, 22, 24).

Another interneuron class, ACs, does not receive direct synaptic input from photoreceptors but from BCs and other ACs (3, 25–28). In mice, there are roughly 60 different AC types. Most ACs act as inhibitory interneurons by releasing GABA or glycine onto BCs, ACs, and RGCs, except for a few glutamatergic and cholinergic AC types, which are also GABAergic cells (3, 23, 29–36). Additionally, a small fraction of interplexiform ACs release dopamine (37–39) and GABA (40) as their neurotransmitters, possibly onto BCs, HCs, and photoreceptors, to conduct synaptic signals from the inner retina to the outer retina.

Identifying each of the retinal cell classes and understanding their synaptic connections is crucial for understanding how the retina processes visual signals. While all the major retinal classes are believed to be defined, we identified a previously undescribed retinal interneuron. This interneuron shares fundamental morphological, physiological, and molecular features with BCs, such as having neurites that ramify in the OPL to receive synaptic inputs from photoreceptors and neurites that project into the IPL to synapse with RGCs. Additionally, this interneuron expresses several common AC markers, and its neurites ramify throughout the entire IPL to synapse with neurons in both ON and OFF IPL. This interneuron may also release the inhibitory neurotransmitter glycine in both the inner and outer retina, in addition to releasing glutamate in the IPL. This atypical retinal interneuron opens the possibility of an anomalous retinal neuron class.

Significance

Cell classes are the building blocks for the central nervous system. It is widely believed that major neuronal classes have been identified in the retina, although some types in the amacrine cell class have not been fully characterized. Here, we describe a retinal interneuron that does not fit into any existing retinal cell class, and we name them Campana cells. Although Campana cells relay visual signals from photoreceptors to the retinal ganglion cells, they differ from bipolar cells in many morphological, physiological, and molecular features. They are also significantly different from amacrine cells. Therefore, our results open the possibility for an unconventional retinal cell class that plays unique roles in visual processing.

Author contributions: B.K.Y. and N.T. designed research; B.K.Y. and N.T. performed research; C.R., T.G., P.W., and K.D. contributed new reagents/analytic tools; B.K.Y. and N.T. analyzed data; B.K.Y. and N.T. wrote the paper; and P.W. managed animal models.

The authors declare no competing interest.

This article is a PNAS Direct Submission. M.B.F. is a guest editor invited by the Editorial Board.

Published under the PNAS license.

[1]To whom correspondence may be addressed. Email: ning.tian@hsc.utah.edu.

This article contains supporting information online at http://www.pnas.org/lookup/suppl/doi:10.1073/pnas.2104884118/-/DCSupplemental.

Published October 26, 2021.

Downloaded at Palestinian Territory, occupied on November 23, 2021

www.manaraa.com

Results

A Transcellular Technique to Label Neurons Synaptically Connected to RGCs. To identify the neurons synaptically connected to RGCs, we developed a transgenic/viral approach to transcellularly label presynaptic neurons of RGCs. This approach utilizes a dual DNA recombinase strategy to express a WGA (wheat germ agglutinin)-Flpo recombinase fused protein in Cre^+ RGCs using a Cre-dependent AAV2-EF1a-DIO-mCherry:IRES-WGA-Flpo viral vector (WGA-Flpo vector, Fig. 1 *A* and *B*) on Cre:FRT-EGFP double transgenic mice (see more details in *SI Appendix*, *Expanded Materials and Methods*). We injected the WGA-Flpo vector into the eyes of CreER-JamB:FRT-EGFP mice. These mice express the Cre DNA recombinase in J-RGCs (41). J-RGCs are OFF-RGCs that activate in response to various light stimulation patterns (41–43). These mice also harbor the R26R CAG-boosted EGFP reporter allele with an *FRT*-flanked STOP cassette in all somatic cells (44). Occasionally, we injected the WGA-Flpo vector into the eyes of CreER-JamB:Thy1-loxP-YFP double transgenic mice to confirm the selective expression of WGA-Flpo in the J-RGCs. The WGA-Flpo vector transduces Cre^+ J-RGCs in these mice and expresses both mCherry and WGA-Flpo–fused proteins (Fig. 1 *B–D*) without transducing retinal neurons in Cre-negative mice at a low titer (4.6×10^{10} vg/mL) (*SI Appendix*, Fig. S1 shows both high and low titers). WGA-Flpo expression in the transduced Cre^+ J-RGCs further induces the expression of mEGFP in these J-RGCs. When WGA-Flpo–fused protein is transported into neurons synaptically connected to the transduced Cre^+ J-RGCs, mEGFP is expressed in these cells, illustrating the cell morphology (Fig. 1 *D–G*).

Using this approach, we examined the types of BCs presynaptic to J-RGCs. In addition to labeling rod BCs (Fig. 1*E*) and OFF cone BCs (Fig. 1*F*), we unexpectedly observed an mEGFP-expressing interneuron that has not been previously described (Fig. 1*G*). Like BCs, this interneuron has neurites that ramify in both the OPL and IPL. However, unlike BCs that stratify their axonal terminals narrowly in either sublamina a (OFF, Fig. 1*F2*) or sublamina b (ON) of the IPL (7, 30, 45), the neurites of this interneuron form multiple branches ramified throughout the entire thickness of the IPL (Fig. 1*G2*). Since this interneuron appears similar to a handbell, with a long neurite that travels to the OPL through the inner nuclear layer (INL; the handle) and broad neuronal ramifications throughout the depth of the IPL (the bell), we call them "Campana cells." *Campana* being Latin for "bell." To better understand this cell, we investigated this interneuron's morphological, biochemical, and physiological properties.

Campana Cells Have Unique Morphological Features. First, we attempted to find a more direct and efficient method to label Campana cells without relying on synaptic transfer. We found that a previously published viral construct, AAV2-CAG-ChR2-GFP-Na1.6 (AAV2-GFP; *SI Appendix*, Fig. S2*A*) (46), can label a variety of different retinal cell types (*SI Appendix*, Fig. S2 *B* and *C*). These include ON cone BCs (type 5 cone BCs; Fig. 2*A*), Campana cells (Fig. 2*B*), and Aii-ACs (Fig. 2*C*).

Using this viral vector, we characterized the morphology of Campana cells in more detail. The Campana cell is typified by having a neural plexus that ramified the entire depth of the IPL and an ascending neurite that reaches the OPL and has large lobules on this ascending process. The OPL projecting neurite is clearly a continuation of a cellular structure from the Campana cell based on the fluorescent labeling with no other labeled cells nearby. This is evident when the image is rotated 90° (Fig. 2*B3*) or in a video showing a 360° rotation (Movie S1). Furthermore, it is striking how similar the Campana cell's neurites in the IPL are to those of Aii-ACs. Therefore, we compared the total length of the neurites of Campana cells with those of Aii-ACs. The results show no significant difference in the length of the neurites in the IPL between Campana cells and Aii-ACs (OFF layer, $P = 0.7456$; ON layer, $P = 0.8692$, unpaired Student's t test; Fig. 2*D*). However, Aii-ACs do not have a neurite that projects to the OPL like the Campana cells (Fig. 2 *C* and *D*).

Campana Cells Receive Synaptic Input from Both Rods and Cones. Next, we determined the Campana cells' synaptic inputs by recording their light-evoked responses. Accordingly, we

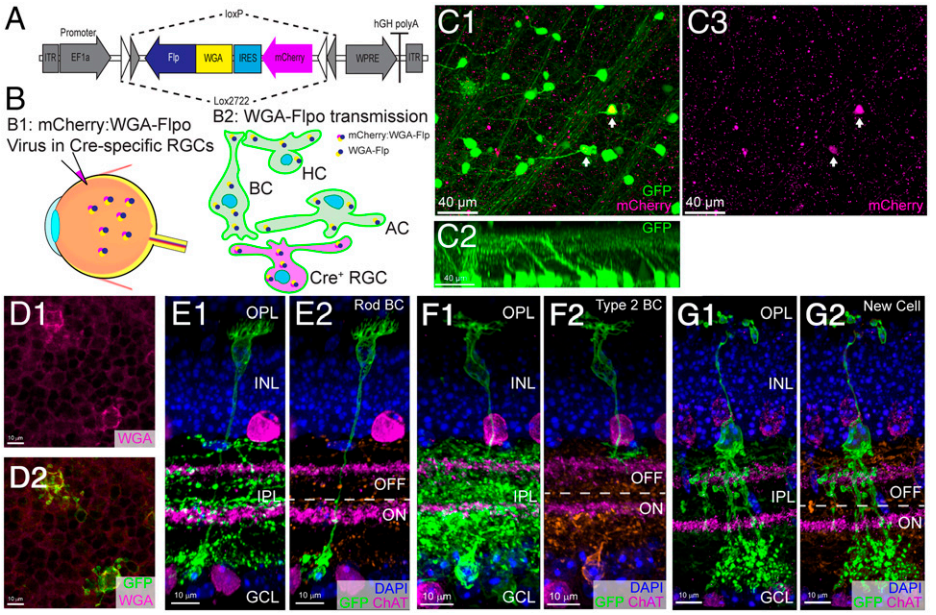

Fig. 1. A transcellular technique to label retinal neurons synaptically connected to RGCs. (*A*) The WGA-Flpo vector. (*B*) Depiction of the use of the WGA-Flpo vector for intraocular injections (*B1*); WGA fused to Flpo expressed by Cre^+ RGCs can be transported from RGCs (magenta) to presynaptic neurons (green; *B2*). (*C*) An image from a flat-mounted retina of a CreER-JamB:Thy1-loxP-YFP double transgenic mouse treated with the WGA-Flpo vector shows many YFP-expressing J-RGCs, in which two of them are $mCherry^+$ J-RGCs (yellow, indicated by white arrows). These cells are YFP^+ (green), and the dendrites project asymmetrically to the OFF layer of the IPL (90° rotation of *C1* is shown in *C2*), indicating that they are J-RGCs. Two cells are also mCherry positive (*C3*, magenta, white arrows), showing that they express the WGA-Flpo vector. (*D*) Anti-WGA staining (*D1*, magenta) in a WGA-Flpo–treated CreER-JamB:FRT-EGFP retina. GFP-positive cells (green) are also WGA-positive (*D2*). (*E*) A rod BC labeled through WGA-Flpo (*E1*) and a masking of the GFP signal shows the morphology (*E2*). Background GFP is color coded in orange, and ChAT (magenta) marks the ON and OFF sublamina. (*F*) A type 2 cone BC labeled through the WGA-Flpo (green) method and colabeled with anti-ChAT (magenta, *F1*) and a masking of the GFP signal from the same cell (*F2*). Background GFP is color coded in orange. (*G*) A morphologically unique cell with neurites that project to both the OPL and IPL labeled through WGA-Flpo (green) and colabeled with ChAT (magenta, *G1*) and a masking of the GFP signal from the same cell (*G2*). Background GFP is color coded in orange.

Downloaded at Palestinian Territory, occupied on November 23, 2021

www.manaraa.com

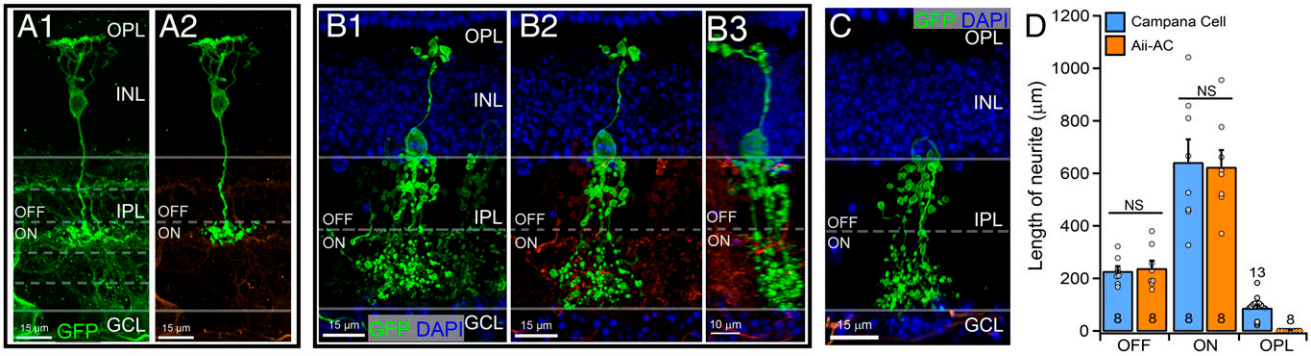

Fig. 2. Campana cells have unique morphological features. (*A*) Image of a type 5 cone BC labeled by the AAV2-GFP vector in a thick (40 μm) retinal cross-section (*A1*, green), and the GFP within the cell masked from the background (orange) to reveal the morphology (*A2*). (*B*) A Campana cell, labeled by AAV2-GFP (*B1*, green) and the same cell (green) masked and isolated from the background (orange, *B2*). *B3* shows the same cell with a 90° rotation about the *y*-axis. (*C*) An Aii-AC labeled by AAV2-GFP. (*D*) A comparison of the mean neurite length of the Campana cell (light blue) and Aii-ACs (orange) in the OFF ($P = 0.7456$, Student's *t* test) and ON ($P = 0.8692$, Student's *t* test) sublamina of IPL shows no significant difference. The ascending neurite of Campana cells has an average length of 88.8 ± 11.9 μm within the OPL. Each dot represents the value of a cell. The number in each column indicates the number of cells. NS: not significant. Error bar: +SE.

generated an AAV2-CAG-GCaMP6m (AAV2-GCaMP6m) viral vector (*SI Appendix*, Fig. S3*A*) to measure the light-evoked changes in the intracellular calcium of Campana cells using a two-photon imaging system (Movie S2 shows an example recording). All recordings were done from the retina's ventral portion, where mice have a high density of ultraviolet (UV)–sensitive s-opsin expressing cones (47). The ventral retina was identified by a higher density of GCaMP6m-labeled cells since the virus vector was injected into the eye's ventral portion (*SI Appendix*, Fig. S3 *B* and *C*).

Fig. 3*A* shows a GCaMP6m-expressing Campana cell from a dark-adapted retina that we used to record the calcium activity of its soma and OPL neurites (Movie S3 shows the cell's image stack). First, we recorded cell responses to both a long (4-s) and a short (10-ms) light flash (Fig. 3 *B* and *C* and reference *SI Appendix*, Fig. S4 and *Expanded Materials and Methods* for details on stimulation protocol). During the 4-s light stimulation, the Campana cell increased its intracellular calcium concentration immediately after the light on, and this continued until the end of the light stimulation (Fig. 3*B*). This result indicates that the Campana cells have a depolarizing response to light. To avoid the light-evoked photomultiplier tube response overlapping with the cell response, we tested a 10-ms light flash stimulation. Surprisingly, the 10-ms light flash also produced a long-lasting response, which continued until slightly before the end of the 30-s recording period (Fig. 3*C*). This lengthy response is the case for 66% of Campana cells (21/32 cells). Fig. 3*D* compares the peak time and amplitudes of light responses evoked by 10-ms and 4-s light flashes from the same group of Campana cells. The results show that the time to peak of the responses to 10-ms light vary significantly among cells while the peak amplitudes of light response to the 4-s light flash vary significantly. Therefore, neither of these two stimuli evoked more consistent results in both the time to peak and amplitude. To minimize the artifact caused by the long light stimulus and prevent photobleaching, we used the 10-ms flash to stimulate the Campana cells in most of our recordings.

To determine the Campana cell's scotopic and photopic properties, we used dim green light and bright UV light flashes (*SI Appendix*, Fig. S5 shows the wavelength distribution; reference *SI Appendix*, *Expanded Materials and Methods* for further details) to stimulate rods and cones, respectively. Fig. 3*E* shows a GCaMP6m-expressing Campana cell from which we recorded light responses from the OPL projecting neurite (box in Fig. 3*E*. Also, Movie S4 shows the cell's image stack). The $\Delta F/F_0$ of the fluorescent intensity of the Campana cell's OPL projecting neurites was plotted as a function of time under these two light conditions (Fig. 3*F*). The data shows that the cell has an increased calcium concentration following the light flash (indicated by the black arrow), which peaks at 8.8/6.5 s (rod/cone) and decays slowly over time. Surprisingly, the kinetics of the Campana cells' light-evoked calcium responses are much slower than those of type 5 cone BCs (Fig. 3 *G* and *H* and Movie S5 shows the image stack). Type 5 cone BCs have a sharp increase in GCaMP6m fluorescence immediately after a light flash (arrow) and reached the peak response at 150 ms after the flash. It returned to baseline in less than 3 s.

Comparing the peak calcium response from the cone BCs and Campana cells demonstrated that most type 5 cone BCs have little to no light response to the dim green light stimulation. In type 5 cone BCs, the median response to the dim green light was 21% of the UV light response (Fig. 3*I*; $P = 0.0028$, Mood's test). The median of the type 5 cone BCs responses to rod stimulation is not statistically different from the baseline noise (Fig. 3*I*; $P = 0.67$, Mood's test). However, two type 5 cone BCs responded to the dim green light stimulation, which is likely due to gap junction connections between the rod and cone photoreceptors or between Aii-ACs and type 5 cone BCs (48, 49). In contrast, Campana cells had an equally robust response to both the dim green and UV light flashes with no significant difference between the two (Fig. 3*I*; $P = 0.066$, Mood's test). When we compared the time of the peak calcium response of type 5 cone BCs and Campana cells, we found that Campana cells reach their peak ~15 times slower than type 5 cone BCs (Fig. 3*J*; $P = 1.2 \times 10^{-4}$, Mood's test).

Campana Cells Primarily Receive Excitatory Synaptic Input through mGluR6. In the vertebrate retina, RGCs and ACs, including interplexiform cells, receive excitatory input from BCs through AMPA/NMDA receptors in the IPL (3, 50). However, BCs receive their primary input from photoreceptors in the OPL. Both rod BCs and ON cone BCs express mGluR6 at their dendritic terminals (15, 16), while OFF cone BCs express both KA (kainic acid) and AMPA (α-amino-3-hydroxy-5-methyl-4-isoxazolepropionic acid) receptors at their dendritic terminals (10).

We sought to determine the primary source of the Campana cells' light-evoked synaptic inputs. Accordingly, we recorded the light responses of Campana cells using calcium imaging with bath application of agonists or antagonists of various glutamate receptor subtypes. Similarly, the Campana cells were

Downloaded at Palestinian Territory, occupied on November 23, 2021

www.manaraa.com

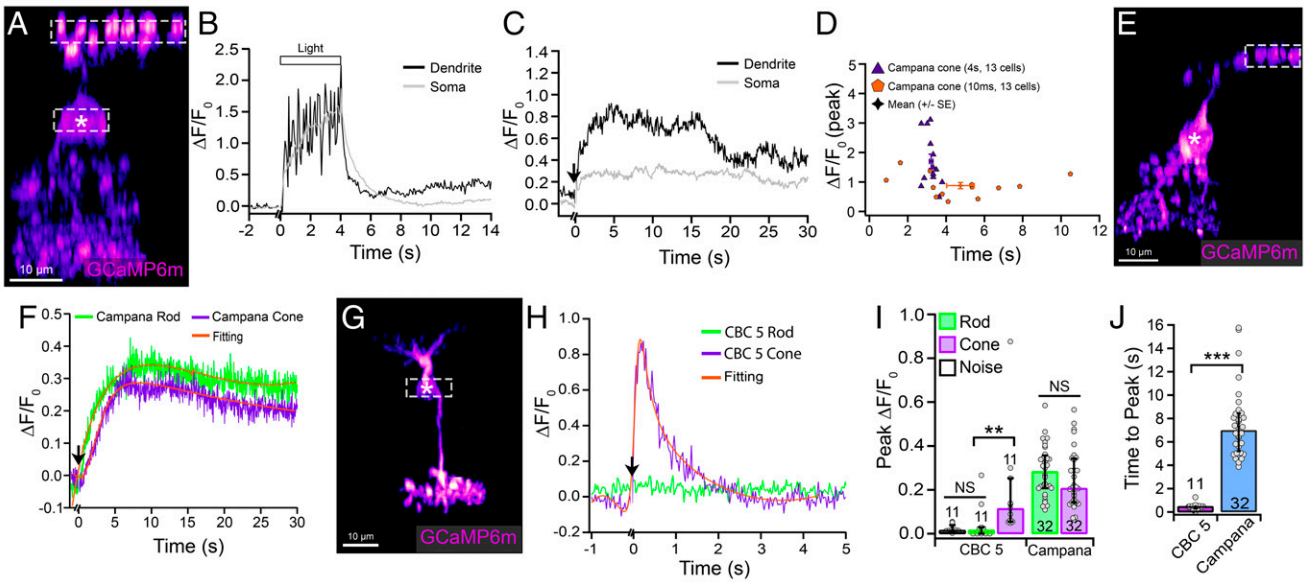

Fig. 3. Campana cells receive synaptic input from both rods and cones. (*A*) An AAV2-GCaMP6m–expressing Campana cell. Its light responses were recorded at its neurites in the OPL and the soma (dashed boxes). (*B*) $\Delta F/F_0$ measured at the OPL terminal (black) and soma (gray) of the Campana cell before, during, and after a 4-s UV light stimulation (white bar above the light response). The response is an average of five traces. (*C*) $\Delta F/F_0$ measured at the OPL terminal (black) and soma (gray) of the Campana cell before, during, and after a 10-ms UV light flash stimulation (black arrow). The response is an average of three traces. (*D*) Scatterplot showing the peak $\Delta F/F_0$ and the time to peak of Campana cell light responses evoked by a 10-ms (orange) and 4-s light stimulus (purple). On average, the light responses evoked by 4-s light have a faster time to peak and a greater amplitude ($P = 0.0244$ and $P = 0.0017$, respectively, paired Student's *t* test, $n = 13$). (*E*) An AAV2-GCaMP6m–expressing Campana cell. Its light responses were recorded at its neurites in the OPL (dashed box). (*F*) $\Delta F/F_0$ measured at the OPL terminal of the Campana cell before, during, and after a 10-ms dim green (green) and UV light (purple) stimulation (black arrow). A 5/4 order polynomial (*SI Appendix, Expanded Materials and Methods*) was used to fit the curves (orange) and measure peak amplitude and time. Responses are averaged from three traces. (*G*) An AAV2-GCaMP6m–expressing type 5 cone BC. We recorded light responses from the soma indicated by the dashed box. (*H*) $\Delta F/F_0$ of the type 5 cone BC (CBC 5) before, during, and after a 10-ms dim green light (green) and UV light (purple) stimulation (black arrow). A polynomial fitting (orange) was used to measure the peak amplitude and time; there was no light response to the rod level light stimulation. (*I*) A comparison of the median peak light response under no light stimulus (noise, black), the dim green (green), and UV (purple) light stimulation in type 5 cone BCs (CBC 5) and Campana cells. Type 5 cone BCs have little to no calcium response to the dim green light stimulation, and it is not significantly greater than noise ($P = 0.670$, Mood's test, $n = 11$). However, the UV light stimulation does generate a significant response ($P = 0.0028$, Mood's test, $n = 11$). In Campana cells, the peak amplitudes of light responses evoked by dim green and UV lights are not statistically different ($P = 0.066$, Mood's test, $n = 32$). Values are shown as median with IQR or middle 50% of the data. (*J*) A comparison of the median time to peak of light responses evoked by a UV light for type 5 cone BCs and Campana cells. A Mood's test showed a significantly longer time to peak for the light response of Campana cells ($P = 1.2 \times 10^{-4}$, $n = 11$ and 32). Values are shown as median (IQR). Cells in *A*, *E*, and *G* were masked from other cells for clarity and rotated 90° from the imaging plane. Somas are indicated by "*" in these panels. Each dot in *I* and *J* represents the value of a cell. The number in each column indicates the number of cells. NS: not significant, $^{**}P = 0.01$ to 0.001, $^{***}P < 0.001$.

identified based on their morphology revealed by GCaMP6m (Fig. 4*A*). We initially found that bath application of an mGluR6 agonist, AP4 (2-amino-4-phosphonobutyrate) (11, 51), wholly and reversibly blocked the light-evoked response of Campana cells (*SI Appendix*, Fig. S6 *A–E*). To determine whether AP4 blocks the light response of Campana cells through other ON BCs indirectly, we further dissected the source of excitatory synaptic inputs to Campana cells. Accordingly, we bath-applied AMPA and NMDA receptor antagonists CNQX (6-Cyano-7-nitroquinoxaline-2,3-dione) and AP5 (DL-2-amino-5-phosphonopentanoic acid) after recording a control response to light flashes (Fig. 4*B*). CNQX+AP5 reduced the maximum $\Delta F/F_0$ amplitude to 71% of the control response for the dim green light stimulation and 53% of the control response for the UV light stimulation. These are significant decreases for both rod- and cone-mediated responses ($P = 0.028$ and 0.00019, respectively; Fig. 4*C*), indicating that Campana cells receive excitatory synaptic inputs through AMPA and NMDA receptors.

Since much of the light response could not be blocked by AMPA/NMDA antagonists, we next determined the role that the mGluR6 played in the Campana cell's light response by bath application of AP4 with AP5 and CNQX. Like AP4 alone, the combination of CNQX+AP5+AP4 eliminated the light response of Campana cells for both the dim green and UV light stimulation (Fig. 4*C*). A wash of 30 to 60 min showed a significant recovery from the CNQX+AP5+AP4 application (Fig. 4*C*). Therefore, Campana cells receive about 71 and 53% of the rod- and cone-mediated light response through mGluR6, respectively. When we compared the effects of CNQX+AP5 on the time to the peak response of Campana cells during both dim green and UV light stimulation, we found that there is no significant change in the time to peak following blockade of AMPA/NMDA receptors (rod, $P = 0.55$; cone, $P = 0.42$; Fig. 4*D*). Therefore, activation of AMPA/NMDA receptors triggers a slow calcium increase in Campana cells, just as mGluR6 does.

To determine whether Campana cells relay their activity to RGCs, we used the AAV2-CAG-ChR2-GFP-Na1.6 vector to express ChR2-GFP in Campana cells and used the red calcium indicator jRGECO1a to record calcium changes (Fig. 4*E*) (46, 52). We activated a single Campana cell by focused laser stimulation in the presence of AP4 to block light-evoked response from rods and cones and recorded responses of the stimulated Campana cells and jRGECO-expressing RGCs (Fig. 4 *E–G*, more than 97% of jRGECO1a positive cells were RGCs; reference *SI Appendix*, Fig. S9*I* for RGC identification and *SI Appendix, Expanded Materials and Methods* for details on the ChR2 experimental protocol). We show that 1-s laser stimulation

Downloaded at Palestinian Territory, occupied on November 23, 2021

www.manaraa.com

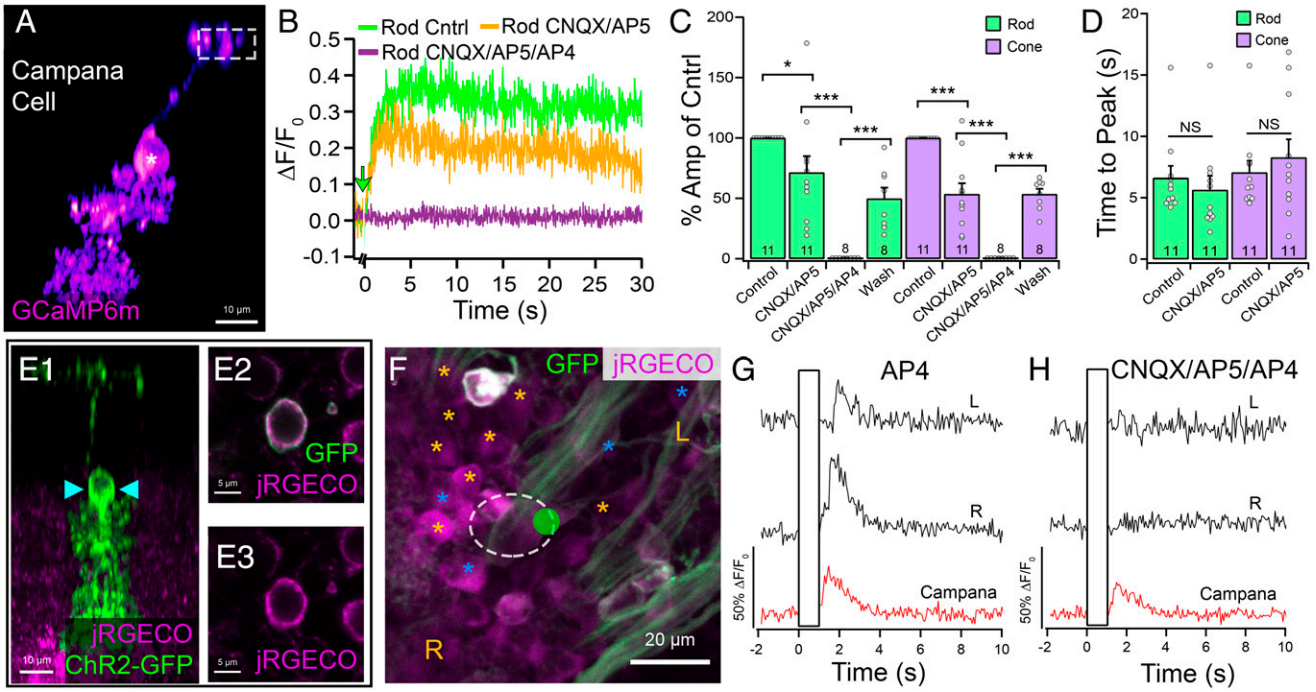

Fig. 4. Campana cells primarily receive excitatory synaptic input through mGluR6 and relay this to the RGC layer. (*A*) An AAV2-GCaMP6m–expressing Campana cell. Its light responses were recorded at its neurite in the OPL (dashed box). (*B*) The change in the light-evoked fluorescent intensity from the Campana cell in *A* before, during, and after a 10-ms dim green light flash (green arrow) in the control condition (green), with bath application of 10 µM CNQX and 35 µM AP5 (orange), and with bath application of 10 µM CNQX, 35 µM AP5, and 50 µM AP4 (purple). Traces are an average of three responses. (*C*) Comparing the effects of CNQX+AP5 or CNQX+AP5+AP4 on the peak calcium light responses of Campana cells during both dim green (green) and UV light (purple) stimulation. All responses were normalized to the maximum response of the control. Drugs were bath-applied in series, and statistical comparisons were made to the previous condition. Rod CNQX+AP5: $P = 0.028$; Rod CNQX+AP5+AP4: $P = 0.00068$; Rod Wash: $P = 0.00047$; Cone CNQX+AP5: $P = 0.00019$; Cone CNQX+AP5+AP4: $P = 0.00097$; Cone Wash: $P = 3.4 \times 10^{-6}$; paired Student's *t* test. ($n = 11$ and 8.) (*D*) A comparison of the effects of CNQX+AP5 on the time to the peak calcium light response of Campana cells during both dim green (green) and UV light (purple) stimulation shows that there is no significant change in time to peak following drug application (Rod: $P = 0.55$; Cone: $P = 0.42$, paired Student's *t* test, $n = 11$). (*E*) An AAV2-ChR2-GFP–expressing Campana cell (green) in a field of jRGECO-expressing cells (magenta). A 473-nm laser stimulation was focused on the soma (teal arrowheads), and the responses were recorded at its soma (*E2* and *E3*). (*F*) Somas in the RGC layer expressing jRGECO (magenta) and ChR2-GFP (green). Only ChR2 negative cells were analyzed. Cells with an increase in calcium signal in response to Campana cell stimulation are colored in orange (L, R, or *) and those that do not are labeled in blue. Corresponding traces for L and R can be seen in *G* and *H*. The dotted oval designates the axonal field area of the Campana cell. (*G*) Response of the Campana cell (red) and two different cells in the RGC layer (black) after laser stimulation of the ChR2-expressing Campana cell. The retina was bathed in Mouse Ringer's containing 50 µM AP4. (*H*) After bath application of CNQX (10 µM)+AP5 (35 µM)+AP4 (50 µM), only the Campana cell still has an increase in its calcium signal. Cells in *A* and *E* were masked from other cells for clarity and rotated 90° from the imaging plane. Each dot in the bar graphs represents the value of a cell. The number in each column indicates the number of cells. NS: not significant, *$P = 0.05$ to 0.01, ***$P < 0.001$.

transiently increased the intracellular calcium of the Campana cell (Fig. 4*G*, red line). In addition, laser stimulation of the Campana cell increased the intracellular calcium of several jRGECO-expressing RGCs (Fig. 4 *F* and *G* and also reference Movie S6 for the kinetics of laser-evoked calcium transients of a Campana cell and RGCs). Bath application of CNQX+AP5+AP4 blocked the laser-induced response of RGCs but not the laser-induced calcium transient of the Campana cell (Fig. 4*H*), indicating Campana cells relay their activity to RGCs through AMPA/NMDA receptors (also reference *SI Appendix*, Fig. S9 for more examples).

Finally, we sought to determine if Campana cells receive their light-evoked synaptic inputs through gap junctions because Aii-ACs depend on gap junction electrical coupling with ON cone BCs to receive light-evoked synaptic inputs (53–56). Our results demonstrate that gap junction coupling has a minimal effect on the light-evoked calcium response of Campana cells (*SI Appendix*, Fig. S6 *F–I*).

Campana Cells Have Close Synaptic Contact with Both Rods and Cones. BCs are divided into rod BCs and cone BCs based on whether they primarily receive synaptic inputs from rods or cones (7, 19, 30, 45). However, our physiological data suggest that Campana cells receive a similar amount of synaptic input from both rods and cones (Fig. 3*I*). We further examined whether Campana cells have direct synaptic connections with rods and cones by examining the proximity of the Campana cell's OPL projecting neurites to rods' and cones' synaptic ribbons. We transfected Campana cells with the AAV2-GFP vector and colabeled the retina with anti-CtBP2 (ribbon protein) (57) and either anti-REEP6 (rods) or anti-cone arrestin (cones) antibodies (58, 59). Using a previously published technique for identifying synaptic contacts (60), we identified the rod or cone synapses that contacted a Campana cell's OPL projecting neurites. Our results showed that the OPL projecting neurites of Campana cells are in proximity (≤300 nm away) with both rod (Fig. 5 *A–D*) and cone synapses (Fig. 5 *E–H*). We confirmed that each cell that we analyzed was a Campana cell by the morphology of its descending and ascending neurites (Fig. 5 *C* and *G*). Statistically, the mean number of contacts between Campana cells and cones is not different from that of rods ($P = 0.38$; Fig. 5*I*). These results support our physiological findings and suggest that the Campana cells likely receive equal synaptic inputs from rods and cones.

Downloaded at Palestinian Territory, occupied on November 23, 2021

www.manaraa.com

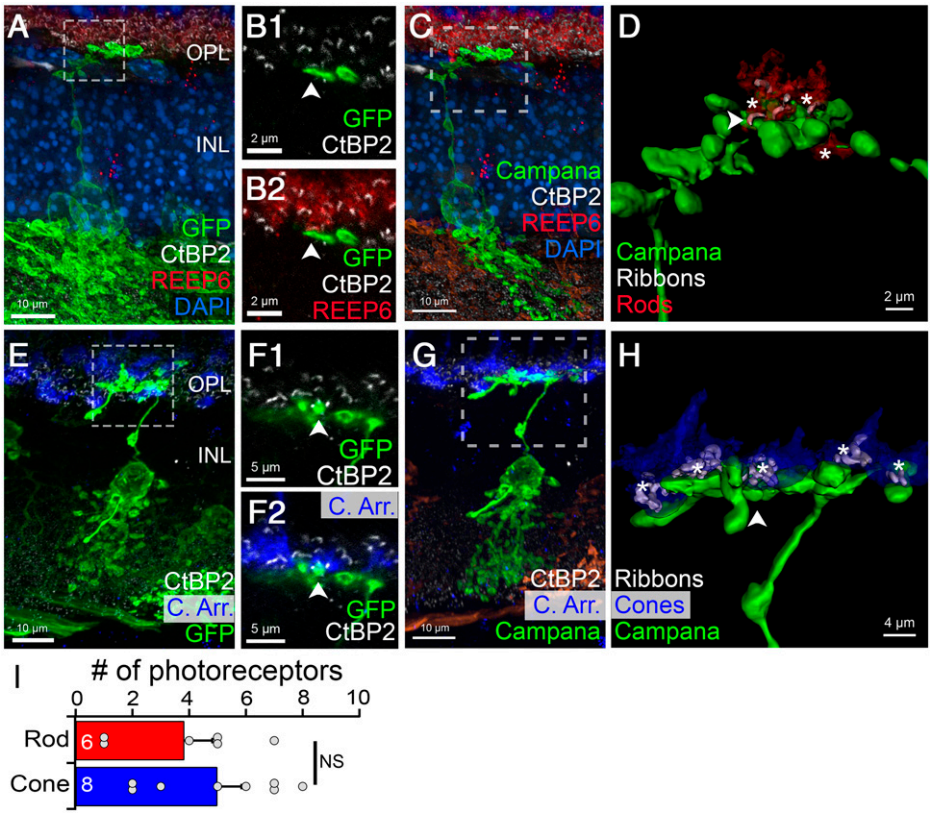

Fig. 5. Campana cells have close synaptic contact with both rods and cones. (*A*) An AAV2-GFP–labeled Campana cell (green) colabeled with anti-REEP6 (rods, red) and anti-CtBP2 (white) antibodies. (*B*) A high-resolution single optic section of the boxed area in *A* shows that the ascending neurite of the Campana cell (green, *B1* and *B2*) is in close contact with a ribbon synapse (white, *B1* and *B2*) in a rod (red, *B2*). (*C*) A masked view of the same Campana cell (green) shown in *A* confirms that it is a Campana cell. (*D*) A surface rendering of the boxed area of *C* shows the Campana cell neurite and rod photoreceptor terminals (red) with ribbon synapses inside (white) that are in close contact with the Campana cell neurite. Asterisks indicate nearby rod terminals, and the arrowhead indicates the neurite segment marked with arrows in *B1* and *B2*. (*E*) An AAV2-GFP–labeled Campana cell (green) colabeled with anti-cone arrestin (cones, blue) and anti-CtBP2 (white) antibodies. (*F*) A high-resolution single optic section of the boxed area in *E* shows that the neurite of the Campana cell (green, *F1* and *F2*) is in close contact with a ribbon synapse (white, *F1* and *F2*) in a cone pedicle (blue, *F2*). (*G*) A masked view of the same Campana cell (green) shown in *E* confirms that it is a Campana cell. (*H*) A surface rendering of the neurite boxed in *G* shows cone photoreceptor terminals (blue) with ribbon synapses inside (white) that are in close contact with the Campana cell dendrite (green). Asterisks indicate individual cone terminals in close contact, and the arrow indicates the dendritic segment of the Campana cell marked with arrows in *F1* and *F2*. (*I*) A comparison of the number of contacts to Campana cell dendrites from cones and rods. The cone contacts are not significantly different from that of rods. Dots represent individual cells, and numbers in each row are the number of cells. NS: not significant.

The Campana Cells Express Some Proteins in Common with BCs. We have shown that the Campana cell has a neurite like a BC dendrite, receives excitatory input through an AP4-sensitive receptor, and has close contact with rod and cone ribbons. We then examined if Campana cells have any protein expression in common with BCs. First, we examined if Campana cells express mGluR6 (61). However, due to the high density of this and other synaptic proteins, we utilized stimulated emission depletion (STED) microscopy to ensure proper colocalization. Fig. 6*A* shows a GFP-expressing Campana cell (green). Super-resolution STED imaging Fig. 6*B*) of the area boxed in Fig. 6*A2* shows proximity between a ribbon synapse in a cone pedicle and mGluR6 in the Campana cell neurite in the OPL. A three-dimensional colocalization analysis confirmed this proximity (Fig. 6*B4*). Because the Campana cells' neurites in the OPL seem to be postsynaptic to photoreceptors with mGluR6, we refer to it as a dendrite.

One feature in common to all BCs is that they use glutamate as their neurotransmitter and use vesicular glutamate transport 1 (VGluT1) to transport glutamate from the cytosol into synaptic vesicles (62). Another feature BCs have in common is the presence of ribbons at their axonal terminals to regulate glutamate release (63, 64). Accordingly, we labeled VGluT1 and ribbons in the mouse retina with anti-VGluT1 (62) and anti-CtBP2 (ribbons) antibodies and determined the localization of ribbons and VGluT1 inside the Campana cell's neurites in the IPL using super-resolution STED imaging (Fig. 6 *C–F*). The resolution of this STED imaging is at least 3 to 4 times higher than the theoretical maximum resolution of standard confocal microscopy (65), and it has been used to illustrate the colocalization of synaptic proteins inside the dendritic and axonal terminals at super-resolution (66–68). Nonetheless, standard confocal microscopy produced similar ribbon colocalization results seen in serial block-face EM (23). Therefore, we refer to the Campana cell's neurites in the IPL as axons and predict that Campana cells may release glutamate through ribbon synapses at their axonal terminals.

In addition, we tested if Campana cells express other common BC-specific antigens. The results show that Campana cells do not express two pan-BC antigens, Vsx2 and Otx2 (*SI Appendix*, Fig. S7 *A* and *B*) (69, 70). Nor do they express the rod BC antigen, PKC (*SI Appendix*, Fig. S7*C*), or the cone BC antigen, CABP5 (*SI Appendix*, Fig. S7*D*) (71).

Campana Cells Express Proteins Commonly Expressed by ACs. Because Campana cells showed substantial morphological similarity to Aii-ACs, we further examined if Campana cells express proteins generally expressed by ACs, especially by Aii-ACs. Our results show that Campana cells are positive for Pax6 (*SI Appendix*, Fig. S8*A*), a paired homeobox gene expressed in ACs, HCs, and RGCs in the mouse retina (70, 72). Additionally, Campana cells are positive for calretinin (*SI Appendix*, Fig. S8*B*), a calcium-binding protein primarily expressed in ACs (73–75). They also express glycine transporter 1 (GlyT1; Fig. 7*A* and Movie S7 shows the cell's image stack), a protein that transports glycine from the extracellular space into cells and is a known marker for Aii-ACs (76).

BCs are excitatory neurons and only release glutamate as their neurotransmitter. However, Campana cells express GlyT1, which would enable Campana cells to transport glycine from the extracellular space into their cytosol. To further determine if Campana cells could load glycine into synaptic vesicles

Downloaded at Palestinian Territory, occupied on November 23, 2021
www.manaraa.com

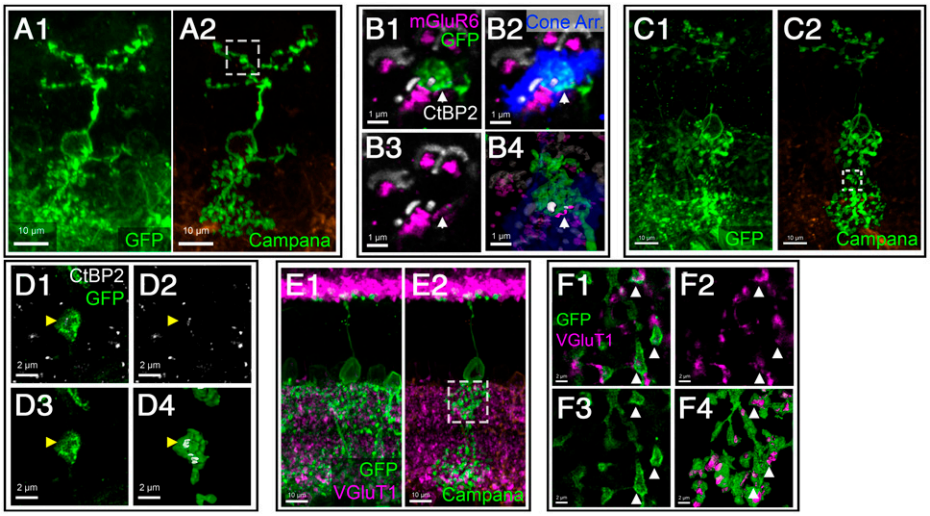

Fig. 6. The Campana cell expresses some proteins in common with BCs. (*A*) An AAV2-GFP–labeled Campana cell (green, *A1*) and a masked view of the same cell in *A1* for clarity (*A2*). (*B*) Three-channel deconvolved STED imaging of the area boxed in *A2* shows a single section of a Campana cell dendrite (green) colabeled by anti-CtBP2 (white) and anti-mGluR6 (magenta) antibodies (*B1–B4*) with 52-nm resolution. Additionally, anti-cone arrestin (blue) was performed at standard confocal resolution (*B2* and *B4*). Anti-mGluR6 antibody-stained puncta (magenta pointed by a white arrow) are located inside the dendritic terminal of the Campana cell (green, *B1*, *B2*, and *B4*) and are closely associated with anti-CtBP2 labeling (white, *B1–B4*) inside a cone terminal (blue, *B2* and *B4*). Three-dimensional (3D) colocalization analysis confirms that mGluR6 is inside the Campana cell dendrite and is closely associated with a cone ribbon synapse (*B4*). (*C*) An AAV2-GFP–labeled Campana cell (green, *C1*). A masked view of the same cell is shown in *C2*. (*D*) Two-channel deconvolved STED imaging (at 56.4-nm resolution) shows a single optic section view of the area indicated by the box in *C2*. Two ribbon synapses (anti-CtBP2, white, one indicated by a yellow arrowhead) are inside the axonal terminal (green) in the IPL (*D1–D4*). A 3D surface rendering (*D4*) shows that the Campana cell's axon envelops the ribbon synapse. (*E*) An AAV2-GFP–labeled Campana cell (green, *E1*) colabeled with anti-VGluT1 (magenta), and a masked view of the same cell is shown in *E2*. (*F*) A two-channel deconvolved STED single optic section view of the area indicated by the box in *E2* shows that VGluT1 (anti-VGluT1, magenta) is colocalized inside the axonal terminal (green, indicated by white arrowheads) in the IPL (*F1–F3*, 126.7-nm resolution). A 3D surface rendering (*F4*) shows that VGluT1 resides throughout the Campana cell's axon.

for release, we examined whether Campana cells express the vesicular inhibitory amino acid transporter (VIAAT/VGAT), which is a membrane transport protein that transports both glycine and GABA from the cytosol into synaptic vesicles (77). When we colabeled AAV2-GFP–transfected Campana cells with anti-VGAT and anti-SV2 antibodies (77–79), we found that every GFP$^+$ Campana cell was VGAT positive and VGAT colocalized with synaptic vesicles labeled by the anti-SV2 antibody (Fig. 7 *B* and *C*). VGAT expression is primarily in the dendritic and axonal terminals of Campana cells (Fig. 7*B* and *SI Appendix*, Fig. S8*C*). While VGAT is always found to be colocalized with SV2, SV2 is not always colocalized with VGAT (Fig. 7*C*), implying that only some synaptic vesicles can load glycine.

Finally, we used an anti-glycine antibody (80) to colabel GFP-expressing Campana cells to determine whether Campana cells contain the neurotransmitter glycine. Our results show that every Campana cell contained glycine. Super-resolution imaging shows that the glycine is concentrated at the dendritic terminals, particularly the varicosity-like structure of Campana

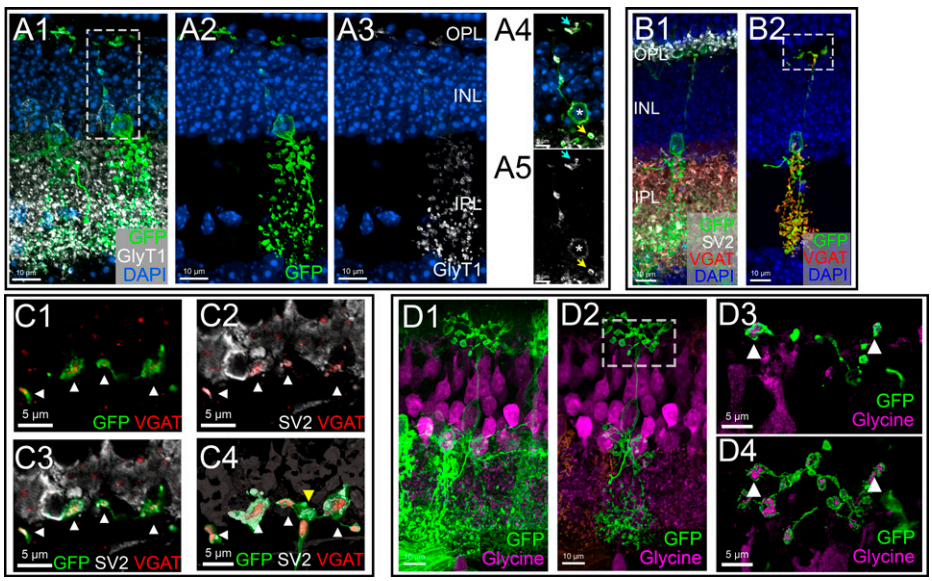

Fig. 7. Campana cells express proteins commonly expressed by ACs. (*A*) An AAV2-GFP–transfected Campana cell (green cell, the right side of *A1*) and Aii-AC (green cell, left side of *A1*) colabeled with anti-GlyT1 antibody (white, *A1* and *A3–A5*). A mask of the Campana cell is shown in *A2*. *A3* shows a mask of the anti-GlyT1 staining within the Campana cell. A single optical frame from the boxed area in *A1* shows that the dendrites (teal arrows), soma (asterisk), and axons (yellow arrows) are GlyT1 positive (white, *A4* and *A5*). (*B*) A Campana cell (green, *B1*) labeled by AAV2-GFP and colabeled with anti-VGAT (red) and anti-SV2 (white) antibodies. *B2* shows a masked view of the same cell in *B1* with GFP and anti-VGAT labeling. (*C*) A single super-resolution optic section of the area boxed in *B2* shows that Campana cell dendrites are positive for SV2 and VGAT (*C1–C4*). (*C1*) GFP and anti-VGAT staining. (*C2*) Anti-SV2 and anti-VGAT. (*C3*) GFP, anti-SV2, and anti-VGAT. (*C4*) A three-dimensional (3D) model of the dendrite shows that VGAT inside the Campana cell terminals colocalizes with SV2 (white arrowheads), however, occasionally SV2 is not colocalized with VGAT (yellow arrowhead). (*D*) A Campana cell (green, *D1*) labeled by AAV2-GFP and colabeled with anti-glycine antibody (magenta, *D1*). (*D2*) A masked view of the Campana cell in *D1*. (*D3*) A deconvolved super-resolution single optic section of the area boxed in *D2* shows that Campana cell dendrites are positive for glycine. (*D4*) A 3D model of the glycine contained within the Campana cell dendrites. Arrowheads indicate the same processes in *D3* and *D4*.

Downloaded at Palestinian Territory, occupied on November 23, 2021

www.manaraa.com

cells (Fig. 7*D*). Additionally, glycine is present in portions of the axon (*SI Appendix*, Fig. S9*K*). These results demonstrated that not only do Campana cells express GlyT1 to transport glycine from the extracellular space into cells and VGAT to transport glycine from the cytosol of the cells into synaptic vesicles, but they also accumulate glycine at their dendritic and axonal terminals. In addition, we found that optogenetic laser activation of Campana cells in the presence of glutamate receptor antagonists induced a decrease of intracellular calcium in some RGCs (*SI Appendix*, Fig. S9). These results support the possibility that Campana cells might release glycine on RGCs. However, BCs do not express VGAT (*SI Appendix*, Fig. S8*E*) or release inhibitory neurotransmitters (30).

Campana cells might also release glycine in the OPL, and the presence of GlyR-α in the OPL has been previously shown (81). Therefore, we used antibody staining to determine what cells express glycine receptor α (GlyR-α) in the OPL. We found that GlyR-α was localized throughout the OPL, including in the dendrites of rod BCs in the OPL, as shown by the colocalization of anti-PKC and anti-GlyRα1 + 2 staining and other locations in OPL (*SI Appendix*, Fig. S8*E*). Therefore, Campana cells could inhibit rod BCs through the activation of their dendritic glycine receptors.

Campana Cells Have a Sparse Retinal Pattern. To determine if Campana cells cover the retina in a uniform pattern, we measured the dendritic and axonal field areas and the Campana cells' density. We obtained dendritic and axonal field area measurements from Campana cells in noncompressed flat-mount retinas from mice labeled with AAV2-GFP. The average dendritic field area is 822 ± 80 μm^2, and the average axonal field area is measured as 598 ± 33 μm^2 (Fig. 8*A*). While the dendritic field size has a large variance, the axonal field size is much more consistent (Fig. 8 *A* and *B*). On average, the Campana cell's dendritic field size is ∼5 times larger than that of rod BCs (33), ∼4 times larger than type 5 cone BCs (P = 0.00136, unpaired Student's t test), ∼7 times larger than type 6 cone BCs, and ∼4 times larger than type 7 cone BCs but roughly equivalent to that of the type 8 cone BCs (82). However, most other studies' measurements were performed on compressed retinal preparations, causing the results to likely be biased to a larger value. Therefore, Campana cells have a much larger dendritic field area than most ON BCs.

Because every AAV2-GFP transduced Campana cell expresses GlyT1 throughout the cell (Fig. 7*A*), and the dendritic field areas of AAV2-GFP transduced Campana cells are not statistically different from the neurite field areas observed in the OPL with anti-GlyT1 labeling (P = 0.708, Mood's test; Fig. 8*A*), we concluded that these GlyT1$^+$ neurites in the OPL belong to Campana cells. Accordingly, we used anti-GlyT1 labeling to estimate Campana cells' density in a noncompressed flat-mount retina of adult mice (Fig. 8*C*). We found that Campana cells have a density of 132 ± 5 cells/mm^2 (mean ± SEM, 953 Campana cells, n = 4 mice).

To determine if the Campana cells have regular spacing, we measured the nearest neighbor (N-N) distance between somas labeled by anti-GlyT1 antibody (Fig. 8*C*, green dots). The mean N-N distance is 55.2 ± 2.91 μm, and the median is 53.2 μm. The N-N probability distribution fits with a Gaussian curve but not a random distribution, indicating nonrandom spacing (Fig. 8*D*) (83). The conformity ratio/regularity index (mean/SD) also supports this conclusion (83, 84). The calculated conformity ratio for Campana cells is 3.35, indicating that Campana cells have a nonrandom distribution in the retina (P < 0.001) (84). However, it has been shown that well-known cell types, such as Aii-ACs, have a random spacing distribution, but Campana cells are spaced much farther apart than a random spacing simulation and have a low density similar to dopaminergic ACs (85).

Campana Cells Are Evolutionarily Conserved in Mammals. Finally, we determined if Campana cells are preserved in other mammals by labeling the retinas of marmosets and macaques with an anti-GlyT1 antibody. Fig. 9*A* shows a macaque retina colabeled by anti-GlyT1 and anti-CtBP2 antibodies. Like mice, the macaque retina contains GlyT1$^+$ cells with dendrites projecting to the OPL and an axonal plexus ramified in both the ON and OFF sublamina of the IPL (Fig. 9*B*). Additionally, the dendrites of the GlyT1$^+$ cell appear to be near the ribbon synapses of both rods and cones (Fig. 9*B*). Similarly, colabeling a marmoset retina using anti-GlyT1 and anti-CtBP2 antibodies revealed GlyT1$^+$ cells with a morphology resembling what we observed in the macaque and mouse retina (Fig. 9 *C* and *D*).

We then used peanut agglutinin (PNA) fused to Alexa 555 to identify cone pedicles in the marmoset retina (Fig. 9*E*) (86). With this approach, we characterized the number of rod and cone ribbon synapses near Campana-like cells' dendrites

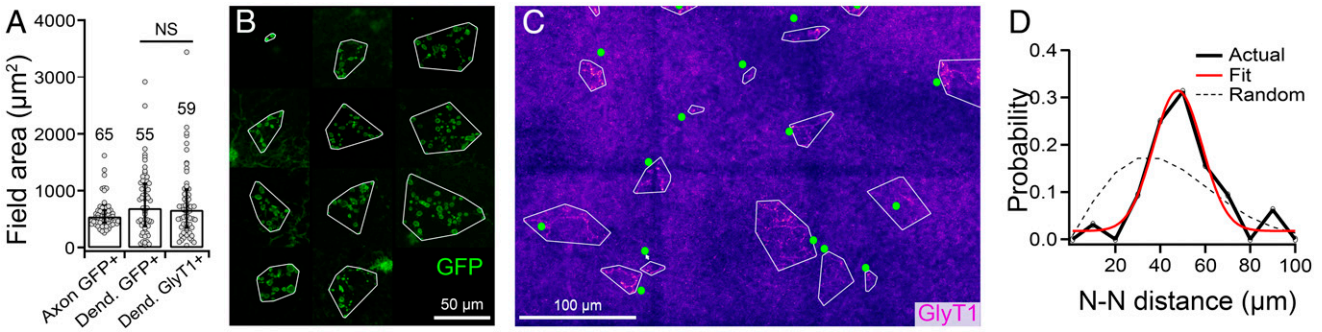

Fig. 8. Campana cells have a sparse retinal pattern. (*A*) The average areas of the dendritic and axonal fields of Campana cells. The dendritic field area measurements were taken from Campana cells in noncompressed flat-mount retinas labeled with anti-GlyT1 antibody (three mice) or AAV2-GFP (six mice). Axonal field area measurements were taken from Campana cells in noncompressed flat-mount retinas labeled with AAV2-GFP (eight mice). Comparing the GFP-labeled dendrites and the GlyT1-labeled dendrites shows no significant difference (P = 0.708, Mood's test). Each dot represents an individual cell. The numbers in each column are the number of cells. Data are represented as median (IQR). NS: not significant. (*B*) A composite view of several different GFP-labeled Campana cell dendrites in the OPL shows the dendritic field area variation. The field area is indicated with a white outline. Cells are ordered from the smallest (top left) to the largest field area (bottom right). (*C*) A view of the OPL of a flat-mount mouse retina shows several Campana cells' dendrites. The field area is indicated with a white outline, and green dots indicate each soma's approximate location. (*D*) A probability distribution function for the N-N distance of each Campana cell soma. The solid black line is the actual observations in bin widths of 10 μm, the solid red line is a normal Gaussian distribution, and the dashed line is a random simulation based on cell density.

Downloaded at Palestinian Territory, occupied on November 23, 2021

www.manaraa.com

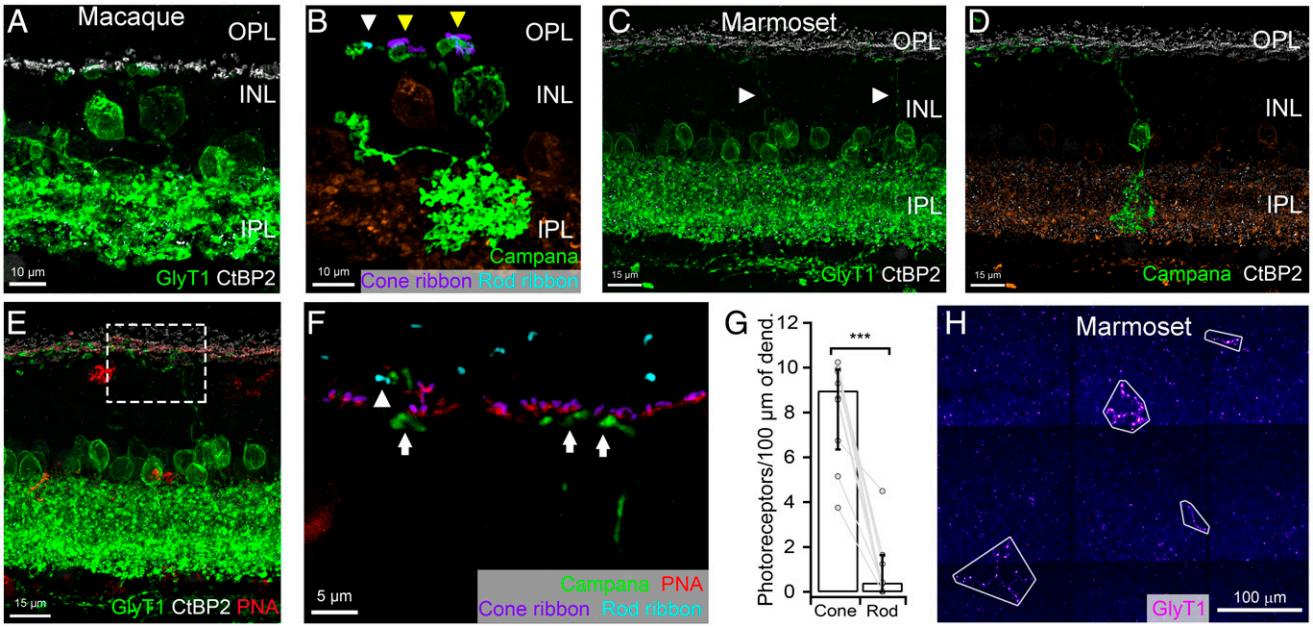

Fig. 9. Campana cells are evolutionarily conserved in mammals. (*A*) A macaque retina labeled with anti-GlyT1 (green) and anti-CtBP2 (white) antibodies. (*B*) The same view in *A* but with the Campana cell masked and isolated (green) from the Aii-ACs (orange). The dendrites show close contact with two cone ribbons (purple, yellow arrowheads) and one rod ribbon (teal, white arrowhead). (*C*) A marmoset retina colabeled with anti-GlyT1 (green) and anti-CtBP2 (white) antibodies shows two Campana cell dendrites (arrowheads). (*D*) The same area in *C* with the leftmost Campana cell (green) masked from the background (orange). (*E*) The same cell on the left in *C* but with CtBP2 (white) to label ribbons and PNA-Alexa555 (red) to label cone terminals. (*F*) A single frame view of the area boxed in *E* and artificially colored shows that the dendrites of the Campana cell have close contacts with both cone ribbons (purple, arrows) and a rod ribbon (teal, arrowhead). (*G*) A comparison of the density of close contacts between the dendrites of Campana cells to rods or cones. A Mood's test shows that the median density of cone contacts is significantly higher than rod contacts ($P = 3.4 \times 10^{-4}$, 10 cells, two marmosets). Data are displayed as median (IQR). Dots represent individual cells, and numbers in each column are the number of cells. ***$P < 0.001$. (*H*) A view of the OPL of a noncompressed flat-mount marmoset retina shows several Campana cells' dendrites. The dendritic field area is outlined with white boundaries.

(Fig. 9*F*). We found that there is a significantly higher density of synaptic contacts with cone ribbons in the primate retina than with rod ribbons ($P = 3.4 \times 10^{-4}$, Mood's test; Fig. 9*G*), likely due to the much higher cone density in the marmoset retina than the mouse retina (87–89). Additionally, marmosets' Campana-like cells have a low density and wide variation in their dendritic field areas, similar to mice (Fig. 9*H*). Collectively, our results demonstrate that Campana cells are preserved across species from mice to primates.

Discussion

What Cell Class Do Campana Cells Belong to? The fundamental findings of this study revealed a previously undescribed retinal interneuron, the Campana cell. This cell shares some essential anatomical, physiological, and biochemical features with BCs, including that the Campana cells ramify dendrites in OPL and axonal terminals in the IPL. Additionally, they express mGluR6 at their dendritic terminals as other ON BCs (15, 16). Also, Campana cells receive light-evoked synaptic inputs directly from photoreceptors and respond to a light stimulus with an increase in intracellular calcium, just as other ON cone BCs and rod BCs do (11, 30, 51). In addition, optogenetic stimulation of Campana cells increases the intracellular calcium concentration of RGCs through glutamate receptors as other BCs (24, 30, 62, 64). Therefore, they primarily function as BCs by relaying visual signals from photoreceptors to RGCs. Furthermore, Campana cells express BC-specific synaptic proteins, such as VGluT1 and CtBP2, at their axonal terminals (30, 57, 62).

However, Campana cells express several unique structural, functional, and biochemical features, which are not present in any BCs and do not follow several principles of the current paradigm of how BCs process visual signals (3). First, BCs are divided into two major groups in all vertebrates based on their synaptic inputs, the rod BCs and cone BCs (30, 90). Under normal conditions, rod BCs predominately synapse with rods, while cone BCs primarily synapse with cones with rare exceptions (3, 19, 23, 30, 91). In contrast, Campana cells synapse with a similar number of rods and cones in the mouse retina. Even in a species with a high cone density, such as marmosets, Campana cells appear to synapse with both rods and cones. Second, BCs stratify their axonal terminals in either the ON or OFF sublamina of the IPL to selectively synapse with either ON or OFF ACs and RGCs (3, 30). However, all Campana cells ramify their axonal terminals throughout the entire IPL to form synapses in both the ON and OFF sublamina, thus crossing the ON–OFF pathway. It has been reported that light-evoked ON responses can be transmitted to OFF pathways as both excitatory and inhibitory synaptic inputs through a "cross-talk" circuit (92, 93). This "cross-talk" is believed to only occur through Aii-ACs and is involved in the rod BC integration into the retinal circuit (27). However, Campana cells may also play a role in this "cross-talk." Third, all BCs are considered excitatory neurons and only release glutamate as their neurotransmitter (24, 30, 62, 64), while Campana cells express transporters for both glutamate (VGluT1) and glycine (VGAT) transvesicular transportation and likely release both glutamate and glycine on RGCs. However, they are not unique in this aspect because VGluT3 ACs and starburst ACs release both excitatory and inhibitory neurotransmitters in a calcium-dependent manner (35, 94, 95). This dual release is achieved through an intracellular system involving synaptic and calcium-dependent regulation for modulating transmitter release (35, 95). Finally, Campana cells do not express several pan-BC markers or BC type-specific markers. Therefore, Campana cells are significantly different from any BC type in many aspects.

Downloaded at Palestinian Territory, occupied on November 23, 2021

www.manaraa.com

Are Campana cells a type of AC? Although Campana cells express several AC-specific markers, such as Pax6, Calretinin, GlyT1, and VGAT, and their axons resemble the morphology of Aii-AC neurites, they are different from ACs in several fundamental aspects. First, Campana cells directly receive synaptic inputs from photoreceptors and relay visual signals to RGCs. Although some ACs, such as dopaminergic interplexiform ACs, project to the OPL from the INL and synapse with HCs and BCs in the OPL, they do not receive direct synaptic input from photoreceptors (50). Indeed, a cell with similar morphology to the Campana cell has been previously observed at least twice in mice and was described as an interplexiform cell (76, 96). However, neither of these studies thoroughly examined the cell's morphological and physiological properties. Second, Campana cells express mGluR6 at their dendritic terminals to relay glutamatergic signals from photoreceptors to the inner retina, while no AC expresses this synaptic receptor in any vertebrate retina. Our physiological and pharmacological results further support this point. Third, Campana cells express synaptic proteins, such as CtBP2 and VGluT1, for glutamate release at their axonal terminals, while no AC, including the group of glutamatergic ACs, expresses these synaptic proteins in any vertebrate retina.

Taken together, Campana cells share some fundamental features with both BCs and ACs but differ significantly from both in many other critical aspects. Because Campana cells have properties that prevent them from being neatly placed into any currently known cell classes in the retina, they are likely to belong to their own unique retinal class. However, one might argue that the dendritic coverage of retinal cells needs to be close or greater than 1 to be defined a cell type, and the dendritic coverage of Campana cells is too low. Although Campana cells have a low density (132 cells/mm^2), they are not unique since several other neuronal types in the retina have a similar or lower density. These include dopaminergic interplexiform ACs (~29 cells/mm^2) (97), GABAergic interplexiform cells (69 cells/mm^2) (40), HCs (135 to 225 cells/mm^2) (83), alpha RGCs (174 cells/mm^2) (83), type 5d/X BC (~800 cells/mm^2), and type 8 BC (~333 cells/mm^2) (9). Accordingly, several identified retinal cell types have their dendritic coverage much smaller than 1. For instance, the estimated sizes of the dendritic field of Type 5d/X and Type 8 cone BCs are 321.55 μm^2 and 804 μm^2, and their densities in the mouse retina are ~800 cells/mm^2 and 333 cells/mm^2, respectively (9, 23). Based on this data, the estimated coverage factors of the dendritic field of these two BC types are ~26% (0.26). Therefore, not all retinal cell types have coverage factors close to 1. In our study, the average dendritic field size of Campana cells and density are 822 ± 80 μm^2 and 132 ± 5 cells/mm^2, respectively. This results in an 11% dendritic coverage of the retina, which is close to that of Type 5d/X and Type 8 cone BCs.

What Role Might Campana Cells Play in Vision? The fundamental question is, what might be the functional role of the Campana cells in visual signal processing? In the vertebrate retina, neuronal circuits process scotopic and photopic vision through rod- and cone-mediated synaptic pathways. Accordingly, rods and cones form synapses with distinct BC types, either rod BCs or cone BCs (7, 19, 30, 45), to process visual signals under scotopic and photopic conditions, respectively (4, 5), and conduct the visual signals to RGCs. Therefore, the first question is whether Campana cells relay their activity to RGCs. Our optogenetic experiments demonstrate that Campana cells relay their activity to RGCs through glutamate receptors. However, Campana cells synapse with both rods and cones. These dual rod/cone inputs enable the Campana cells to transmit light responses of both rods and cones to RGCs but prevents Campana cells from distinguishing these signals. It is unclear how this capability would benefit visual signal processing.

In addition, the slow kinetics of the light-evoked response of Campana cells will limit their temporal resolution for image-forming vision. These kinetics are similar to those of ipRGCs, which have light responses that can last for tens of seconds after the end of light stimulation (98). Similarly, persistent firing neurons have been found in the postsubiculum, amygdala, entorhinal cortex, piriform cortex, and prefrontal cortex in mice, rats, and primates (99–104). Mechanistically, ipRGCs and other persistent firing neurons have been found to rely on metabotropic glutamate receptors to receive synaptic inputs, with ipRGCs expressing the group III receptor mGluR7 and neurons in the central nervous system (CNS) expressing group I mGluRs 1/5 (101, 103, 105). Additionally, hyperpolarization-activated cyclic nucleotide-gated channels (HCN) have also been shown to play a role in generating persistent firing (104).

In the retina, mGluR7 causes a sustained depolarization in ipRGCs by providing positive feedback after the end of glutamate release from cone BCs (105). In the CNS, mGluR1/5 works through the second messenger IP3 to release internal calcium stores and possibly activate HCN channels (106, 107). However, ON BCs express mGluR6, a group III receptor (15), which responds to glutamate release from photoreceptors within milliseconds (14). mGluR6 works through the G protein complex $G\alpha_0$ to ultimately open the nonselective cation channel transient receptor potential melanoma-related 1 (TRPM1) (108–110). Nevertheless, this molecular pathway has not been reported to cause a persistent increase in intracellular calcium concentration.

Our results strongly support that Campana cells rely on mGluR6 for their light-evoked intracellular calcium responses. Additionally, the molecular pathways to relay the mGluR6 signaling to the intracellular calcium release in Campana cells seem different from those found in ON BCs. Interestingly, pharmacological blockade of AMPA and NMDA receptors reduced the amplitude of light-evoked intracellular calcium responses of Campana cells without changing the kinetics. This result indicates that activation of AMPA/NMDA receptors also triggers a slow calcium increase in Campana cells like mGluR6, although both AMPA and NMDA receptors have fast channel kinetics. Therefore, Campana cells are more likely to have a unique activity-dependent mechanism for intracellular calcium regulation. This mechanism requires further investigation.

What can the role of persistent firing neurons reveal about the function of Campana cells? In the retina, ipRGCs are involved in various non-image-forming processes such as pupil dilation and circadian photoentrainment (111). In the CNS, persistent firing cells in the entorhinal cortex are believed to be involved in memory and learning (112) and ones in the postsubiculum are thought to maintain head position information over time (102). Therefore, it would be interesting to investigate whether Campana cells play a role in non-image-forming vision, such as acting as a low-pass frequency filter or maintaining a temporally regulated "memory" of a recent stimulation.

Materials and Methods

For a more detailed description of materials and methods, reference *SI Appendix*.

Animals. Adult wild-type C57BL/6 mice, CreER-JamB:FRT-EGFP double transgenic, and CreER-JamB:Thy1-loxP-YFP double transgenic mice with a C57BL/6 background of either sex were used in this study. All animal procedures and care were performed following protocols approved by the Institutional Animal Care and Use Committee of the University of Utah in compliance with Public Health Service guidelines.

Virus Injections. Four AAV viral vectors were used in this study, AAV2-EF1a-DIO-mCherry:IRES-WGA-Flpo, AAV2-CAG-ChR2-GFP-Na1.6, AAV2-CAG-GCaMP6m, and AAV1-Syn-jRGECO1a. All injections were performed under anesthesia.

Downloaded at Palestinian Territory, occupied on November 23, 2021
www.manaraa.com

WGA-Flpo Technique. CreER-JamB:FRT-EGFP mice were injected with tamoxifen at a young age (P7-P14) and then the WGA-Flpo virus was injected 1 wk later. Mice were euthanized 8 to 12 wk following virus injection.

Immunohistochemistry. A detailed antibody staining procedure and the antibodies used can be found in *SI Appendix*.

Image Acquisition and Analysis. Noncompressed, flat-mount retinas were imaged using a two-photon (Bruker) or a Zeiss LSM 700 or 800 microscope. Super-resolution microscopy was performed using Zeiss Airyscan or Leica SP8 X.

Two-Photon Calcium Imaging and Light Stimulation. Calcium imaging was performed on retinas that had been injected with AAV2-GCaMP6m or AAV1-jRGECO1a on the ventral side. Ex vivo recordings were performed while the retina was perfused with Mouse Ringer's bubbled with carbogen (95% O_2, 5% CO_2). An array of light-emitting diodes provided light stimulation, and a focused 473-nm laser was used for ChR2 excitation. Curve fitting was performed on the calcium responses as described in *SI Appendix*. In $\Delta F/F_0$, F_0 is the initial fluorescent intensity, and ΔF is the difference between the fluorescence intensity from each time point and F_0.

Statistical Analysis. All data were tested for normal distribution using the Shapiro–Wilk test. Nonparametric tests were used for data that were not normally distributed. The statistical test performed is stated in the figure legends. Data are reported as mean ± SEM or median (interquartile range [IQR]), and all graphs use +SEM or IQR for error bars. Data were analyzed and organized using Microsoft Excel, XLSTAT (Addinsoft), and Igor (Wavemetrics).

Data Availability. The AAV2-EF1a-DIO-mCherry:IRES-WGA-Flpo virus is available from the UNC Vector Core (Catalog No.: AV6255). To obtain the AAV2-CAG-GCaMP6m virus, please contact Wayne State University Technology Commercialization (telephone: 313-577-5655, email: ttoinfo@wayne.edu). All data related to the paper are included in the article and/or in the *SI Appendix*.

ACKNOWLEDGMENTS. This work was supported by NIH Grants R01EY012345 (N.T.), R01EY031699 (N.T.), T32EY024234 (B.K.Y.), and by HHMI (K.D.). Additional support was provided by NIH Core Grant (EY014800) and an Unrestricted Grant from Research to Prevent Blindness to the Department of Ophthalmology & Visual Sciences, University of Utah, and the Department of Ophthalmology of Wayne State University School of Medicine (T.G.). T.G. received support from the Ligon Research Center of Vision, Kresge Eye Institute, Dryer Foundation. We want to thank Dr. Joshua Sanes for the J-RGC mouse line, Dr. Alessandra Angelucci for the primate retinal tissue, Dr. Botir T. Sagdullaev for the anti-GlyT1, Dr. Catherine W. Morgans for the anti-mGluR6, and Dr. Anand Swaroop for the anti-REEP6. We want to thank Dr. Zhuo-Hua Pan for the AAV2-GFP and AAV2-GCaMP6m viral construct. STED microscopy was performed at the Advanced Light Microscopy/Spectroscopy Laboratory and the Leica Microsystems Center of Excellence at the California NanoSystems Institute at the University of California, Los Angeles with funding support from NIH Shared Instrumentation Grant S10OD025017 and NSF Major Research Instrumentation Grant CHE-0722519. We thank Dr. Laurent Bentolila for assistance with STED microscopy.

1. H. Asari, M. Meister, Divergence of visual channels in the inner retina. *Nat. Neurosci.* **15**, 1581–1589 (2012).
2. T. Gollisch, M. Meister, Eye smarter than scientists believed: Neural computations in circuits of the retina. *Neuron* **65**, 150–164 (2010).
3. R. H. Masland, The neuronal organization of the retina. *Neuron* **76**, 266–280 (2012).
4. S. A. Bloomfield, B. Völgyi, The diverse functional roles and regulation of neuronal gap junctions in the retina. *Nat. Rev. Neurosci.* **10**, 495–506 (2009).
5. F. A. Dunn, R. O. L. Wong, Wiring patterns in the mouse retina: Collecting evidence across the connectome, physiology and light microscopy. *J. Physiol.* **592**, 4809–4823 (2014).
6. T. D. Lamb, Why rods and cones? *Eye (Lond.)* **30**, 179–185 (2016).
7. H. Wässle, C. Puller, F. Müller, S. Haverkamp, Cone contacts, mosaics, and territories of bipolar cells in the mouse retina. *J. Neurosci.* **29**, 106–117 (2009).
8. R. Azeredo da Silveira, B. Roska, Cell types, circuits, computation. *Curr. Opin. Neurobiol.* **21**, 664–671 (2011).
9. M. Helmstaedter *et al.*, Connectomic reconstruction of the inner plexiform layer in the mouse retina. *Nature* **500**, 168–174 (2013).
10. S. H. DeVries, Bipolar cells use kainate and AMPA receptors to filter visual information into separate channels. *Neuron* **28**, 847–856 (2000).
11. M. M. Slaughter, R. F. Miller, 2-amino-4-phosphonobutyric acid: A new pharmacological tool for retina research. *Science* **211**, 182–185 (1981).
12. S. Nawy, C. E. Jahr, Suppression by glutamate of cGMP-activated conductance in retinal bipolar cells. *Nature* **346**, 269–271 (1990).
13. S. Nawy, C. E. Jahr, cGMP-gated conductance in retinal bipolar cells is suppressed by the photoreceptor transmitter. *Neuron* **7**, 677–683 (1991).
14. R. A. Shiells, G. Falk, Glutamate receptors of rod bipolar cells are linked to a cyclic GMP cascade via a G-protein. *Proc. Biol. Sci.* **242**, 91–94 (1990).
15. Y. Nakajima *et al.*, Molecular characterization of a novel retinal metabotropic glutamate receptor mGluR6 with a high agonist selectivity for L-2-amino-4-phosphonobutyrate. *J. Biol. Chem.* **268**, 11868–11873 (1993).
16. A. Nomura *et al.*, Developmentally regulated postsynaptic localization of a metabotropic glutamate receptor in rat rod bipolar cells. *Cell* **77**, 361–369 (1994).
17. O. S. Dhande, B. K. Stafford, J. A. Lim, A. D. Huberman, Contributions of retinal ganglion cells to subcortical visual processing and behaviors. *Annu. Rev. Vis. Sci.* **1**, 291–328 (2015).
18. C. Pandarinath, J. D. Victor, S. Nirenberg, Symmetry breakdown in the ON and OFF pathways of the retina at night: Functional implications. *J. Neurosci.* **30**, 10006–10014 (2010).
19. C. Behrens, T. Schubert, S. Haverkamp, T. Euler, P. Berens, Connectivity map of bipolar cells and photoreceptors in the mouse retina. *eLife* **5**, e20041 (2016).
20. S. H. Lindstrom, D. G. Ryan, J. Shi, S. H. DeVries, Kainate receptor subunit diversity underlying response diversity in retinal off bipolar cells. *J. Physiol.* **592**, 1457–1477 (2014).
21. S. Saszik, S. H. DeVries, A mammalian retinal bipolar cell uses both graded changes in membrane voltage and all-or-nothing Na^+ spikes to encode light. *J. Neurosci.* **32**, 297–307 (2012).
22. K. Shekhar *et al.*, Comprehensive classification of retinal bipolar neurons by single-cell transcriptomics. *Cell* **166**, 1308–1323.e30 (2016).
23. L. Della Santina *et al.*, Glutamatergic monopolar interneurons provide a novel pathway of excitation in the mouse retina. *Curr. Biol.* **26**, 2070–2077 (2016).
24. T. Baden, P. Berens, M. Bethge, T. Euler, Spikes in mammalian bipolar cells support temporal layering of the inner retina. *Curr. Biol.* **23**, 48–52 (2013).
25. J. E. Dowling, B. B. Boycott, Organization of the primate retina: Electron microscopy. *Proc. R. Soc. Lond. B Biol. Sci.* **166**, 80–111 (1966).
26. J. S. Kim *et al.*; EyeWirers, Space-time wiring specificity supports direction selectivity in the retina. *Nature* **509**, 331–336 (2014).
27. C. W. Graydon *et al.*, Synaptic transfer between rod and cone pathways mediated by AII amacrine cells in the mouse retina. *Curr. Biol.* **28**, 2739–2751.e3 (2018).
28. W. Yan *et al.*, Mouse retinal cell atlas: Molecular identification of over sixty amacrine cell types. *J. Neurosci.* **40**, 5177–5195 (2020).
29. W. Wei, A. M. Hamby, K. Zhou, M. B. Feller, Development of asymmetric inhibition underlying direction selectivity in the retina. *Nature* **469**, 402–406 (2011).
30. T. Euler, S. Haverkamp, T. Schubert, T. Baden, Retinal bipolar cells: Elementary building blocks of vision. *Nat. Rev. Neurosci.* **15**, 507–519 (2014).
31. R. H. Masland, The fundamental plan of the retina. *Nat. Neurosci.* **4**, 877–886 (2001).
32. M. A. MacNeil, R. H. Masland, Extreme diversity among amacrine cells: Implications for function. *Neuron* **20**, 971–982 (1998).
33. P. W. Keeley, B. E. Reese, Role of afferents in the differentiation of bipolar cells in the mouse retina. *J. Neurosci.* **30**, 1677–1685 (2010).
34. J. Johnson *et al.*, Vesicular glutamate transporter 3 expression identifies glutamatergic amacrine cells in the rodent retina. *J. Comp. Neurol.* **477**, 386–398 (2004).
35. S. Lee, K. Kim, Z. J. Zhou, Role of ACh-GABA cotransmission in detecting image motion and motion direction. *Neuron* **68**, 1159–1172 (2010).
36. D. M. O'Malley, J. H. Sandell, R. H. Masland, Co-release of acetylcholine and GABA by the starburst amacrine cells. *J. Neurosci.* **12**, 1394–1408 (1992).
37. C. R. Jackson *et al.*, Retinal dopamine mediates multiple dimensions of light-adapted vision. *J. Neurosci.* **32**, 9359–9368 (2012).
38. A. G. Knapp, J. E. Dowling, Dopamine enhances excitatory amino acid-gated conductances in cultured retinal horizontal cells. *Nature* **325**, 437–439 (1987).
39. P. Witkovsky, Dopamine and retinal function. *Doc. Ophthalmol.* **108**, 17–40 (2004).
40. K. Dedek *et al.*, A novel type of interplexiform amacrine cell in the mouse retina. *Eur. J. Neurosci.* **30**, 217–228 (2009).
41. I.-J. Kim, Y. Zhang, M. Yamagata, M. Meister, J. R. Sanes, Molecular identification of a retinal cell type that responds to upward motion. *Nature* **452**, 478–482 (2008).
42. M. Joesch, M. Meister, A neuronal circuit for colour vision based on rod-cone opponency. *Nature* **532**, 236–239 (2016).
43. A. Nath, G. W. Schwartz, Electrical synapses convey orientation selectivity in the mouse retina. *Nat. Commun.* **8**, 2025 (2017).
44. V. H. Sousa, G. Miyoshi, J. Hjerling-Leffler, T. Karayannis, G. Fishell, Characterization of Nkx6-2-derived neocortical interneuron lineages. *Cereb. Cortex* **19** (suppl. 1), i1–i10 (2009).
45. Y. Tsukamoto, N. Omi, Classification of mouse retinal bipolar cells: Type-specific connectivity with special reference to rod-driven AII amacrine pathways. *Front. Neuroanat.* **11**, 92 (2017).
46. C. Wu, E. Ivanova, J. Cui, Q. Lu, Z.-H. Pan, Action potential generation at an axon initial segment-like process in the axonless retinal AII amacrine cell. *J. Neurosci.* **31**, 14654–14659 (2011).
47. A. Ortín-Martínez *et al.*, Number and distribution of mouse retinal cone photoreceptors: Differences between an albino (Swiss) and a pigmented (C57/BL6) strain. *PLoS One* **9**, e102392 (2014).
48. S. A. Bloomfield, R. F. Dacheux, Rod vision: Pathways and processing in the mammalian retina. *Prog. Retin. Eye Res.* **20**, 351–384 (2001).

NEUROSCIENCE

Downloaded at Palestinian Territory, occupied on November 23, 2021

www.manaraa.com

49. M. R. Deans, B. Volgyi, D. A. Goodenough, S. A. Bloomfield, D. L. Paul, Connexin36 is essential for transmission of rod-mediated visual signals in the mammalian retina. *Neuron* **36**, 703–712 (2002).
50. J. E. Dowling, *The Retina: An Approachable Part of the Brain* (The Belknap Press of Harvard University Press, Revised Edition, 2012).
51. R. A. Shiells, G. Falk, S. Naghshineh, Action of glutamate and aspartate analogues on rod horizontal and bipolar cells. *Nature* **294**, 592–594 (1981).
52. H. Dana *et al.*, Sensitive red protein calcium indicators for imaging neural activity. *eLife* **5**, e12727 (2016).
53. M. L. Veruki, E. Hartveit, AII (Rod) amacrine cells form a network of electrically coupled interneurons in the mammalian retina. *Neuron* **33**, 935–946 (2002).
54. M. L. Veruki, E. Hartveit, Meclofenamic acid blocks electrical synapses of retinal AII amacrine and ON-cone bipolar cells. *J. Neurophysiol.* **101**, 2339–2347 (2009).
55. K. Dedek *et al.*, Localization of heterotypic gap junctions composed of connexin45 and connexin36 in the rod pathway of the mouse retina. *Eur. J. Neurosci.* **24**, 1675–1686 (2006).
56. E. Hartveit, M. L. Veruki, Electrical synapses between AII amacrine cells in the retina: Function and modulation. *Brain Res.* **1487**, 160–172 (2012).
57. F. Schmitz, A. Königstorfer, T. C. Südhof, RIBEYE, a component of synaptic ribbons: A protein's journey through evolution provides insight into synaptic ribbon function. *Neuron* **28**, 857–872 (2000).
58. C. Liu, H. Bakeri, T. Li, A. Swaroop, Regulation of retinal progenitor expansion by Frizzled receptors: Implications for microphthalmia and retinal coloboma. *Hum. Mol. Genet.* **21**, 1848–1860 (2012).
59. S. Veleri *et al.*, REEP6 mediates trafficking of a subset of Clathrin-coated vesicles and is critical for rod photoreceptor function and survival. *Hum. Mol. Genet.* **26**, 2218–2230 (2017).
60. E. Strettoi, R. A. Masri, U. Grünert, AII amacrine cells in the primate fovea contribute to photopic vision. *Sci. Rep.* **8**, 16429 (2018).
61. C. W. Morgans, G. Ren, L. Akileswaran, Localization of nyctalopin in the mammalian retina. *Eur. J. Neurosci.* **23**, 1163–1171 (2006).
62. D. M. Sherry, M. M. Wang, J. Bates, L. J. Frishman, Expression of vesicular glutamate transporter 1 in the mouse retina reveals temporal ordering in development of rod vs. cone and ON vs. OFF circuits. *J. Comp. Neurol.* **465**, 480–498 (2003).
63. R. W. West, Light and electron microscopy of the ground squirrel retina: Functional considerations. *J. Comp. Neurol.* **168**, 355–377 (1976).
64. T. Baden, T. Euler, M. Weckström, L. Lagnado, Spikes and ribbon synapses in early vision. *Trends Neurosci.* **36**, 480–488 (2013).
65. C. L. Smith, "Basic confocal microscopy" in *Current Protocols in Molecular Biology*, F. M. Ausubel *et al.*, Eds. (John Wiley & Sons, Inc., 2008), pp. 14.11.1–14.11.18.
66. B. van Bommel, A. Konietzny, O. Kobler, J. Bär, M. Mikhaylova, F-actin patches associated with glutamatergic synapses control positioning of dendritic lysosomes. *EMBO J.* **38**, e101183 (2019).
67. C. P. Frias *et al.*, Semaphorin4D induces inhibitory synapse formation by rapid stabilization of presynaptic boutons via MET coactivation. *J. Neurosci.* **39**, 4221–4237 (2019).
68. Y. Fukata *et al.*, LGI1-ADAM22-MAGUK configures transsynaptic nanoalignment for synaptic transmission and epilepsy prevention. *Proc. Natl. Acad. Sci. U.S.A.* **118**, e2022580118 (2021).
69. D. Baas *et al.*, The subcellular localization of Otx2 is cell-type specific and developmentally regulated in the mouse retina. *Brain Res. Mol. Brain Res.* **78**, 26–37 (2000).
70. T. Belecky-Adams *et al.*, Pax-6, Prox 1, and Chx10 homeobox gene expression correlates with phenotypic fate of retinal precursor cells. *Invest. Ophthalmol. Vis. Sci.* **38**, 1293–1303 (1997).
71. U. Grünert, P. R. Martin, H. Wässle, Immunocytochemical analysis of bipolar cells in the macaque monkey retina. *J. Comp. Neurol.* **348**, 607–627 (1994).
72. R. E. Hill *et al.*, Mouse small eye results from mutations in a paired-like homeobox-containing gene. *Nature* **354**, 522–525 (1991).
73. R. Gábriel, P. Witkovsky, Cholinergic, but not the rod pathway-related glycinergic (AII), amacrine cells contain calretinin in the rat retina. *Neurosci. Lett.* **247**, 179–182 (1998).
74. S. C. Massey, S. L. Mills, Antibody to calretinin stains AII amacrine cells in the rabbit retina: Double-label and confocal analyses. *J. Comp. Neurol.* **411**, 3–18 (1999).
75. J. H. Rogers, Calretinin: A gene for a novel calcium-binding protein expressed principally in neurons. *J. Cell Biol.* **105**, 1343–1353 (1987). Correction in: *J. Cell Biol.* **110**, 1845 (1990).
76. S. Haverkamp, H. Wässle, Immunocytochemical analysis of the mouse retina. *J. Comp. Neurol.* **424**, 1–23 (2000).
77. S. L. McIntire, R. J. Reimer, K. Schuske, R. H. Edwards, E. M. Jorgensen, Identification and characterization of the vesicular GABA transporter. *Nature* **389**, 870–876 (1997).
78. Q.-F. Wan *et al.*, SV2 acts via presynaptic calcium to regulate neurotransmitter release. *Neuron* **66**, 884–895 (2010).
79. F. Weltzien, C. Puller, G. A. O'Sullivan, I. Paarmann, H. Betz, Distribution of the glycine receptor β-subunit in the mouse CNS as revealed by a novel monoclonal antibody. *J. Comp. Neurol.* **520**, 3962–3981 (2012).
80. D. V. Pow, L. L. Wright, D. I. Vaney, The immunocytochemical detection of amino-acid neurotransmitters in paraformaldehyde-fixed tissues. *J. Neurosci. Methods* **56**, 115–123 (1995).
81. L. Heinze, R. J. Harvey, S. Haverkamp, H. Wässle, Diversity of glycine receptors in the mouse retina: Localization of the α4 subunit. *J. Comp. Neurol.* **500**, 693–707 (2007).
82. F. A. Dunn, R. O. L. Wong, Diverse strategies engaged in establishing stereotypic wiring patterns among neurons sharing a common input at the visual system's first synapse. *J. Neurosci.* **32**, 10306–10317 (2012).
83. H. Wässle, H. J. Riemann, The mosaic of nerve cells in the mammalian retina. *Proc. R. Soc. Lond. B Biol. Sci.* **200**, 441–461 (1978).
84. J. E. Cook, Spatial properties of retinal mosaics: An empirical evaluation of some existing measures. *Vis. Neurosci.* **13**, 15–30 (1996).
85. P. W. Keeley, S. J. Eglen, B. E. Reese, From random to regular: Variation in the patterning of retinal mosaics. *J. Comp. Neurol.* **528**, 2135–2160 (2020).
86. J. C. Blanks, L. V. Johnson, Specific binding of peanut lectin to a class of retinal photoreceptor cells. A species comparison. *Invest. Ophthalmol. Vis. Sci.* **25**, 546–557 (1984).
87. C.-J. Jeon, E. Strettoi, R. H. Masland, The major cell populations of the mouse retina. *J. Neurosci.* **18**, 8936–8946 (1998).
88. A. D. Springer, D. Troilo, D. Possin, A. E. Hendrickson, Foveal cone density shows a rapid postnatal maturation in the marmoset monkey. *Vis. Neurosci.* **28**, 473–484 (2011).
89. A. K. Goodchild, K. K. Ghosh, P. R. Martin, Comparison of photoreceptor spatial density and ganglion cell morphology in the retina of human, macaque monkey, cat, and the marmoset *Callithrix jacchus*. *J. Comp. Neurol.* **366**, 55–75 (1996).
90. S. Haverkamp, F. Haeseleer, A. Hendrickson, A comparison of immunocytochemical markers to identify bipolar cell types in human and monkey retina. *Vis. Neurosci.* **20**, 589–600 (2003).
91. H. Kolb, Organization of the outer plexiform layer of the primate retina: Electron microscopy of Golgi-impregnated cells. *Philos. Trans. R. Soc. Lond. B Biol. Sci.* **258**, 261–283 (1970).
92. J.-J. Pang, F. Gao, S. M. Wu, Cross-talk between ON and OFF channels in the salamander retina: Indirect bipolar cell inputs to ON-OFF ganglion cells. *Vision Res.* **47**, 384–392 (2007).
93. C. Zhang, M. A. McCall, Receptor targets of amacrine cells. *Vis. Neurosci.* **29**, 11–29 (2012).
94. K. Yoshida *et al.*, A key role of starburst amacrine cells in originating retinal directional selectivity and optokinetic eye movement. *Neuron* **30**, 771–780 (2001).
95. S. Lee, Y. Zhang, M. Chen, Z. J. Zhou, Segregated glycine-glutamate co-transmission from vGluT3 amacrine cells to contrast-suppressed and contrast-enhanced retinal circuits. *Neuron* **90**, 27–34 (2016).
96. L. J. Fisher, Interplexiform cell of the mouse retina: A Golgi demonstration. *Invest. Ophthalmol. Vis. Sci.* **18**, 521–523 (1979).
97. M. Sankaran, P. W. Keeley, L. He, P. M. Iuvone, B. E. Reese, Dopaminergic amacrine cell number, plexus density, and dopamine content in the mouse retina: Strain differences and effects of Bax gene disruption. *Exp. Eye Res.* **177**, 208–212 (2018).
98. J. L. Ecker *et al.*, Melanopsin-expressing retinal ganglion-cell photoreceptors: Cellular diversity and role in pattern vision. *Neuron* **67**, 49–60 (2010).
99. W. A. Suzuki, E. K. Miller, R. Desimone, Object and place memory in the macaque entorhinal cortex. *J. Neurophysiol.* **78**, 1062–1081 (1997).
100. A. V. Egorov, K. Unsicker, O. von Bohlen und Halbach, Muscarinic control of graded persistent activity in lateral amygdala neurons. *Eur. J. Neurosci.* **24**, 3183–3194 (2006).
101. M. Yoshida, E. Fransén, M. E. Hasselmo, mGluR-dependent persistent firing in entorhinal cortex layer III neurons. *Eur. J. Neurosci.* **28**, 1116–1126 (2008).
102. M. Yoshida, M. E. Hasselmo, Persistent firing supported by an intrinsic cellular mechanism in a component of the head direction system. *J. Neurosci.* **29**, 4945–4952 (2009).
103. V. L. Navaroli, Y. Zhao, P. Boguszewski, T. H. Brown, Muscarinic receptor activation enables persistent firing in pyramidal neurons from superficial layers of dorsal perirhinal cortex. *Hippocampus* **22**, 1392–1404 (2012).
104. S. J. Thuault *et al.*, Prefrontal cortex HCN1 channels enable intrinsic persistent neural firing and executive memory function. *J. Neurosci.* **33**, 13583–13599 (2013).
105. X. Zhao *et al.*, Mechanisms creating transient and sustained photoresponses in mammalian retinal ganglion cells. *J. Gen. Physiol.* **149**, 335–353 (2017).
106. S. Ashhad, D. Johnston, R. Narayanan, Activation of $InsP_3$ receptors is sufficient for inducing graded intrinsic plasticity in rat hippocampal pyramidal neurons. *J. Neurophysiol.* **113**, 2002–2013 (2015).
107. S. A. Neymotin *et al.*, Calcium regulation of HCN channels supports persistent activity in a multiscale model of neocortex. *Neuroscience* **316**, 344–366 (2016).
108. K. Weng *et al.*, Functional coupling of a human retinal metabotropic glutamate receptor (hmGluR6) to bovine rod transducin and rat G_o in an *in vitro* reconstitution system. *J. Biol. Chem.* **272**, 33100–33104 (1997).
109. C. Koike *et al.*, TRPM1 is a component of the retinal ON bipolar cell transduction channel in the mGluR6 cascade. *Proc. Natl. Acad. Sci. U.S.A.* **107**, 332–337 (2010).
110. K. A. Martemyanov, A. P. Sampath, The transduction cascade in retinal ON-bipolar cells: Signal processing and disease. *Annu. Rev. Vis. Sci.* **3**, 25–51 (2017).
111. M. Hatori *et al.*, Inducible ablation of melanopsin-expressing retinal ganglion cells reveals their central role in non-image forming visual responses. *PLoS One* **3**, e2451 (2008). Correction in: *PLoS One*, 10.1371/journal.pone.0002451 (2008).
112. C. Lin, V. N. Sherathiya, M. M. Oh, J. F. Disterhoft, Persistent firing in LEC III neurons is differentially modulated by learning and aging. *eLife* **9**, e56816 (2020).

Downloaded at Palestinian Territory, occupied on November 23, 2021

www.manaraa.com